LETTERS

nature cell biology

Synergy between XMAP215 and EB1 increases microtubule growth rates to physiological levels

Marija Zanic[1], Per O. Widlund[1], Anthony A. Hyman[1] and Jonathon Howard[1,2]

In cells, a complex network of proteins regulates the dynamic growth of microtubules that is essential for division and migration. *In vitro* approaches with purified components have so far been unable to reconstitute fast microtubule growth observed *in vivo*[1–3]. Here we show that two well-studied plus-end-binding proteins—end-tracking protein EB1 and microtubule polymerase XMAP215—act together to strongly promote microtubule growth to cellular rates. Unexpectedly, the combined effects of XMAP215 and EB1 are highly synergistic, with acceleration of growth well beyond the product of the individual effects of either protein. The synergistic growth promotion does not rely on any of the canonical EB1 interactions, suggesting an allosteric interaction through the microtubule end. This hypothesis is supported by the finding that taxol and XMAP215, which have non-overlapping binding sites on tubulin, also act synergistically on growth. The increase in growth rates is accompanied by a strong enhancement of microtubule catastrophe by EB1, thereby rendering the fast and dynamic microtubule behaviour typically observed in cells[2,4–6].

Among dozens of plus-end-binding proteins, several stand out for their ability to autonomously track the growing microtubule end[1,7]. Two notable examples are XMAP215 family and EB family proteins. XMAP215 is a microtubule-associated protein that enhances microtubule growth rates up to tenfold[8–10]. Individual XMAP215 molecules remain bound to growing plus ends during multiple rounds of tubulin dimer addition; they also bind to shrinking plus ends[9]. In contrast, EB1 transiently binds to both plus and minus ends of growing, but not shrinking, microtubules[3,5,11–13]. EB1 has also been reported to promote microtubule growth[6,14–16]; however, the main role of EB1 is thought to be in recruiting other plus-end-binding proteins to the growing microtubule end region[17].

Although XMAP215 strongly increases microtubule growth rates, it cannot account, on its own, for the high growth rates observed in cells. For example, growth rates of 10–20 $\mu m\,min^{-1}$ are observed in many cells[2,4–6], yet the highest growth rates observed *in vitro* with XMAP215 are still several-fold lower. As it has been reported that XMAP215 and EB1 interact in frog egg extracts[18], we wondered whether they modulate each other's microtubule-regulating activities at the end. To address this question, we investigated the growth and shrinkage of microtubules using total internal reflection fluorescence (TIRF) microscopy[19]. Growth of green tubulin extensions from red stabilized microtubule seeds was observed in the presence and absence of unlabelled EB1 and unlabelled XMAP215 (see Methods). Figure 1a shows representative kymographs of individual growth events in different assay conditions: whereas XMAP215 alone increased the growth rate, as seen by the increased slope of the kymograph (Fig. 1a, upper right panel) when compared with the tubulin-alone control (Fig. 1a, upper left panel), EB1 alone had little effect on growth rate, although it strongly promoted switching from microtubule growth to shrinkage (microtubule catastrophe; Fig. 1a, lower left panel). The combination of EB1 and XMAP215 had a very strong effect on growth rate (Fig. 1a, lower right panel), much larger than the effect of XMAP215 alone.

To quantify the effects of EB1 on microtubule growth in the presence of XMAP215, we performed a titration in EB1 concentration from 0 to 800 nM, using a fixed concentration of tubulin and XMAP215 (5 μM tubulin and 200 nM XMAP215, the concentration at which the effect of XMAP215 on growth rates is saturated[9,10]). We observed a fourfold promotion of microtubule growth rates, from $4.96 \pm 0.27\,\mu m\,min^{-1}$ (s.e.m., $n = 23$) at 0 nM EB1, to $19.03 \pm 0.63\,\mu m\,min^{-1}$ (s.e.m., $n = 26$) at 800 nM EB1 (Fig. 1b). The effect of EB1 saturates (Fig. 1b, symbols), and is well fitted by a standard enzyme kinetics relation (smooth curve), as predicted by our catalytic model (see Methods). We also investigated the effects of XMAP215 and EB1 over a range of tubulin concentrations, between 3 and 9 μM, in the presence of saturating concentrations of XMAP215 and EB1 (200 nM XMAP215 and 400 nM EB1). Addition of EB1 in combination with XMAP215 led to a boost in microtubule growth rates at all investigated tubulin concentrations (Fig. 1c), yielding rates up to $20\,\mu m\,min^{-1}$, with an increase of

[1]Max Planck Institute of Molecular Cell Biology and Genetics, Pfotenhauerstraße 108, 01307 Dresden, Germany.
[2]Correspondence should be addressed to J.H. (e-mail: howard@mpi-cbg.de)

Received 1 August 2012; accepted 2 April 2013; published online 12 May 2013; DOI: 10.1038/ncb2744

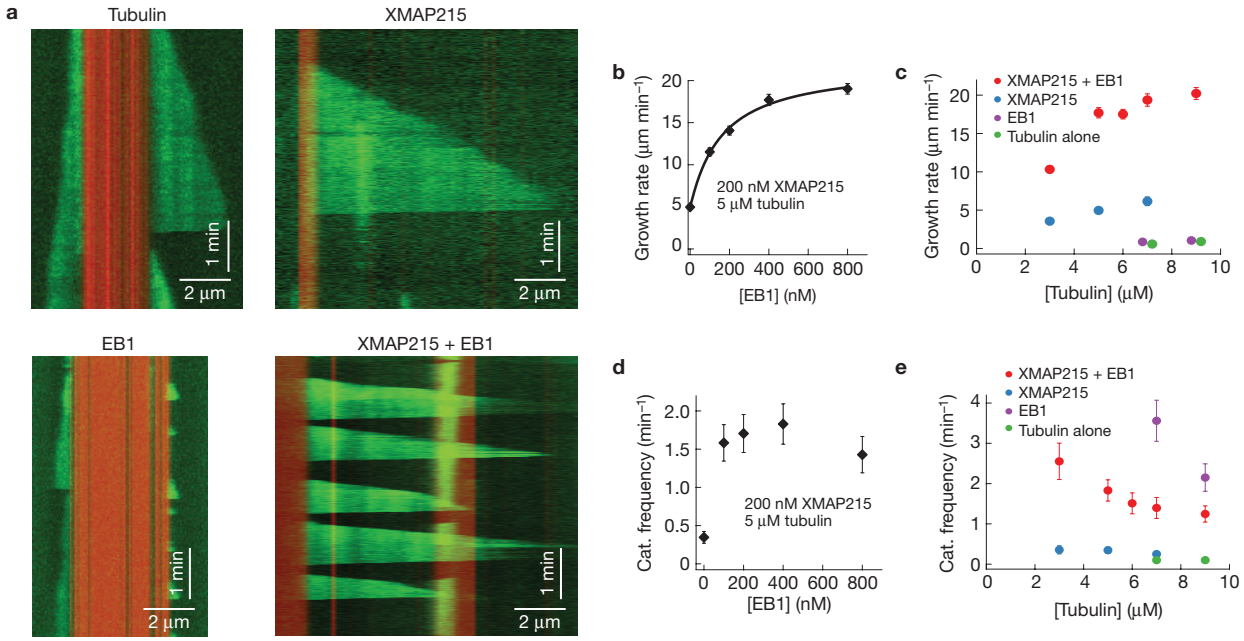

Figure 1 EB1 and XMAP215 synergistically regulate microtubule dynamics. (**a**) Kymographs showing typical microtubule growth events with free tubulin alone, free tubulin with XMAP215, free tubulin with EB1, and free tubulin with both EB1 and XMAP215. Green Alexa488-labelled tubulin extensions are growing out of red tetrarhodamine-labelled, GMPCPP-stabilized microtubule seeds. Microtubule plus ends are on the right. (**b**) Microtubule growth rates as a function of EB1 concentration in the presence of a fixed amount of free tubulin (5 µM) and XMAP215 (200 nM). Error bars represent the s.e.m. $n = 23, 26, 29, 28, 26$ independent measurements of individual growth events in 3 independent experiments for each condition. The line is a fit to the Hill equation: $v([EB1]) = v_0 + (v_{max} - v_0)[EB1]^n/(K^n + [EB1]^n)$, where $n = 1.04 \pm 0.35$ represents the Hill coefficient, v_0 is the growth rate in the absence of EB1, $v_{max} = 21.9 \pm 3.0\,\mu m\,min^{-1}$ is the saturating growth rate and $K = 160 \pm 62$ nM is the concentration of EB1 at half-maximum rate. (**c**) Microtubule growth rates as a function of tubulin concentration for a series of conditions involving a fixed amount of EB1 (400 nM) and/or XMAP215 (200 nM). Data points for EB1 and tubulin alone are offset horizontally for better viewing. Error bars represent the s.e.m. Tubulin with XMAP215 and EB1 (red): $n = 18(2), 28(3), 27(3), 18(3), 32(3)$; tubulin with XMAP215 (blue): $n = 12(2), 23(3), 33(3)$; tubulin with EB1 (purple): $n = 19(3), 30(3)$; tubulin alone (green): $n = 17(3), 21(3)$ independent measurements of individual growth events. Number of independent experiments for each condition is given in parentheses. (**d**) Microtubule catastrophe frequency as a function of EB1 concentration in the presence of a fixed amount of free tubulin (5 µM) and XMAP215 (200 nM). Error bars represent the s.e.m. $n = 20, 44, 47, 48, 36$ individual catastrophe events observed over 3 independent experiments for each condition. (**e**) Microtubule catastrophe frequency as a function of tubulin concentration for a series of conditions involving a fixed amount of EB1 (400 nM) and/or XMAP215 (200 nM). Error bars represent the s.e.m. Tubulin with XMAP215 and EB1 (red): $n = 32(2), 48(3), 34(3), 29(3), 38(3)$; tubulin with XMAP215 (blue): $n = 12(2), 20(3), 31(3)$; tubulin with EB1 (purple): $n = 48(3), 40(3)$; tubulin alone (green): $n = 15(3), 18(3)$ individual catastrophe events observed. Number of independent experiments for each condition is given in parentheses. See Supplementary Table S1 for data.

up to 33-fold when compared with the growth of tubulin alone (Supplementary Table S1; compare data at 7 µM tubulin). These rates obtained with EB1 and XMAP215 represent, to the best of our knowledge, the highest microtubule growth rates ever observed outside cells.

Interestingly, in the absence of XMAP215, EB1 had only a mild effect on microtubule growth rates (Fig. 1c), consistent with previous reports[12,15,20]. In our assay conditions, no microtubule growth was observed with 5 µM tubulin alone, and the addition of 400 nM EB1 did not result in any observable microtubule growth. Furthermore, at higher tubulin concentrations (7 and 9 µM), at which addition of tubulin alone leads to persistent growth of extensions, addition of EB1 resulted in at most a 50% increase in microtubule growth rates, well below the fourfold increase observed when EB1 was added in the presence of XMAP215. We conclude that XMAP215 and EB1 act in synergy to promote microtubule growth, as their combined effect on microtubule growth rate (up to 33-fold) is much greater than the product of their individual effects (up to 10-fold for XMAP215 and up to 1.5-fold for EB1).

In addition to the strong enhancement of microtubule growth rates, we observed that EB1 increases the incidence of microtubule catastrophe in all of our experimental conditions (Fig. 1d,e). In the presence of 5 µM tubulin and 200 nM XMAP215, a titration in EB1 concentration led to a fivefold increase in catastrophe frequency from $0.35 \pm 0.08\,min^{-1}$ (s.e.m., $n = 20$) for no added EB1, to $1.83 \pm 0.26\,min^{-1}$ for 400 nM EB1 (s.e.m., $n = 48$, Fig. 1d). On its own, addition of EB1 led to a 30-fold increase in catastrophe frequency (from $0.10 \pm 0.03\,min^{-1}$ (s.e.m., $n = 15$) with 7 µM tubulin, to $3.56 \pm 0.51\,min^{-1}$ (s.e.m., $n = 48$) with 7 µM tubulin and 400 nM EB1, Fig. 1e and Supplementary Table S1), whereas increasing the tubulin concentration slightly reduced the catastrophe frequency in all experimental conditions (Fig. 1e). Thus, EB1 is a strong catastrophe factor, in the presence and absence of XMAP215.

EB1 is known to play an important role in targeting its partner proteins to the growing microtubule plus end[3,11,12,17]. Therefore, we wondered whether the synergistic action of EB1 with XMAP215 could be a consequence of enhanced end targeting of XMAP215 through an interaction with EB1. However, the finding that the synergy occurs at saturating concentrations of XMAP215 argues against enhanced targeting: in the absence of EB1, an increase in XMAP215 concentration above 200 nM does not lead to further enhancement of growth[9], and

the rates observed with EB1 and XMAP215 together have never been achieved by the action of XMAP215 alone. Thus, it is not expected that simply targeting more XMAP215 to growing microtubule ends would result in such a pronounced enhancement of microtubule growth rates.

Even though the synergy does not arise through enhanced end targeting of XMAP215 by EB1, it is possible that a direct interaction between EB1 and XMAP215 is still necessary for the observed promotion of microtubule growth. To investigate this possibility we performed a series of experiments. First, we removed the last 20 amino acids at the carboxy terminus of EB1, reported to be involved in the interaction of EB1 and XMAP215 (refs 14,18), and known to be necessary for all characterized interactions of EB1 with its partner proteins[17]. We found that this construct (EB1ΔC) did not significantly enhance the microtubule growth in the absence of XMAP215 (Supplementary Table S2), similar to the full-length EB1. Also like full-length EB1, in the presence of XMAP215, EB1ΔC increased the growth rate fourfold (from $4.45 \pm 0.13\,\mu m\,min^{-1}$ (s.e.m., $n = 30$) with no EB1ΔC to $17.02 \pm 0.49\,\mu m\,min^{-1}$ (s.e.m., $n = 36$) with EB1ΔC, Fig. 2a). Thus, this deletion did not disrupt the synergistic effect on microtubule growth rates, indicating that the synergy is not due to the canonical EB1 protein interactions.

In a second experiment to investigate the interaction between EB1 and XMAP215, we studied the localization of EB1 and XMAP215 in the presence of each other on dynamic microtubule ends. On its own, EB1 binds growing, but not shrinking, microtubule ends[3,5,11–13,21], whereas XMAP215 binds to the microtubule plus end irrespective of its dynamic state (growth or shrinkage)[9]. If the direct interaction between the two proteins is involved in their synergistic effect on microtubule growth, both proteins might exhibit the same localization in the presence of each other. However, XMAP215–GFP retained its plus-end binding to shrinking ends in the presence of EB1 (Fig. 2b, left panel), whereas EB1–GFP dissociated from the shrinking end even in the presence of XMAP215 (Fig. 2b, right panel). Thus, the two proteins do not affect each other's localization, at least at this resolution.

Finally, we performed size-exclusion chromatography using full-length EB1, in combination with XMAP215, in the standard buffer conditions used in our TIRF assay. The experiment revealed no sign of direct interaction between the two full-length proteins (Fig. 2c). This is consistent with recent reports that the interaction between EB1 and XMAP215 is mediated by the proteins SLAIN2 (ref. 22) and Sentin[23], and could explain why the pulldown assays in *Xenopus* extracts, where all binding partners are expected to be present, showed binding of EB1 to XMAP215 (ref. 18). Therefore, we conclude that the observed synergistic effect of EB1 and XMAP215 on microtubule growth rates is not a consequence of formation of a complex of the two proteins before binding the microtubule end.

Our finding that the synergy does not depend on the direct interaction between EB1 and XMAP215 implies that the effect occurs through the combined action of the two proteins that takes place only at the growing microtubule end. A recent paper[24] reported that TOG domains, which are tubulin-binding domains of XMAP215 necessary for its polymerase activity[10], preferentially bind the curved conformation of tubulin dimers. The authors propose that the release of the end-bound tubulin dimer by XMAP215, needed for the processive addition of multiple rounds of tubulin dimers by a single XMAP215 molecule, occurs after the end-bound dimer straightens due to its

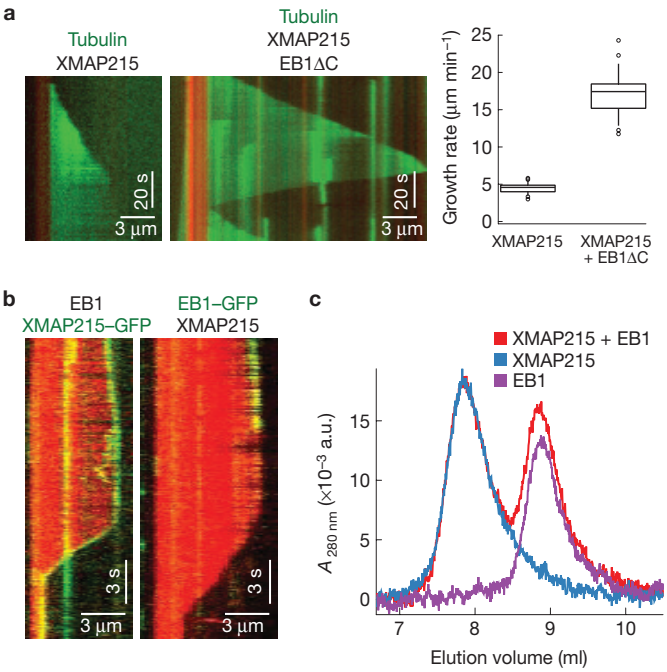

Figure 2 Synergy is not a consequence of a direct interaction between EB1 and XMAP215. (**a**) Kymographs showing typical microtubule growth events with 5 μM free tubulin and 200 nM XMAP215 in the absence (left) and presence (middle) of 400 nM EB1ΔC. Green Alexa488-labelled tubulin extensions are growing out of red tetrarhodamine-labelled, GMPCPP-stabilized microtubule seeds. Microtubule growth rates in the absence and presence of 400 nM EB1ΔC (right). In each box, the mid-line shows the median value, the top and bottom show the upper and lower quartiles (the 75th and 25th percentiles), and the whiskers show the 90th and 10th percentiles. Outliers (extreme 5 percentiles) are represented with round markers. $n = 30$ (without EB1ΔC) and 36 (with EB1ΔC) independent measurements of individual growth events in 3 independent experiments for each condition. (**b**) Kymographs showing the end localization of XMAP215–GFP in the presence of red tetrarhodamine-labelled tubulin and unlabelled EB1 (left), and the end localization of EB1–GFP in the presence of red tetrarhodamine-labelled tubulin and unlabelled XMAP215 (right). (**c**) $A_{280\,nm}$ absorbance as a function of elution volume from the size-exclusion chromatography experiments. Three traces are shown: XMAP215 alone (blue), EB1 alone (purple), and a mixture of XMAP215 and EB1 (red).

incorporation into the microtubule lattice. We therefore reasoned that EB1 accelerates the polymerase activity of XMAP215 by straightening protofilaments at the microtubule end through enhancement of lateral interactions between neighbouring tubulin dimers[15,21,25].

If the synergistic effect of XMAP215 and EB1 on microtubule growth is realized through straightening of tubulin dimers by EB1 at the microtubule end, we expected that taxol, which has been shown to induce protofilament straightening[26], should also exhibit synergistic effects on growth rates when combined with XMAP215. To test this hypothesis, we investigated the growth of microtubules in our assay in the presence of taxol (Fig. 3). We found that taxol strongly suppresses microtubule catastrophe and does not enhance microtubule growth rates with tubulin alone. However, when added in combination with XMAP215, taxol induced further promotion of growth rates (from $3.44 \pm 0.13\,\mu m\,min^{-1}$ (s.e.m., $n = 30$) with no taxol to 6.21 ± 0.33 with 10 μM taxol (s.e.m., $n = 30$), $P < 0.0001$), showing synergistic behaviour with XMAP215, implying that the synergy can be accomplished through modulation of the microtubule structure. Furthermore, because the

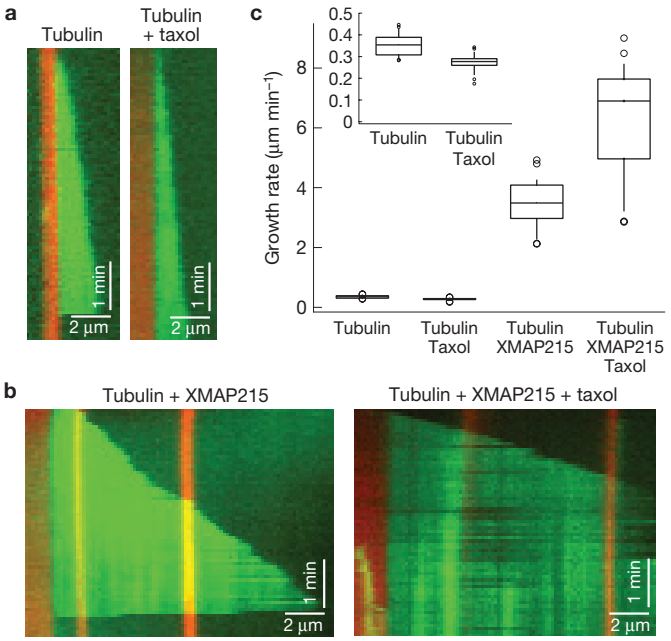

Figure 3 Synergistic promotion of growth can also be achieved by XMAP215 in combination with taxol. (**a**) Kymographs showing typical microtubule growth events with 6 μM free tubulin in the absence (left) and presence (right) of 10 μM taxol. Green Alexa488-labelled tubulin extensions are growing out of red tetrarhodamine-labelled, GMPCPP-stabilized microtubule seeds. (**b**) Kymographs showing typical microtubule growth events with 6 μM free tubulin and 200 nM XMAP215 in the absence (left) and presence (right) of 10 μM taxol. (**c**) Microtubule growth rates in the absence and presence of taxol. In each box, the mid-line shows the median value, the top and bottom show the upper and lower quartiles (the 75th and 25th percentiles), and the whiskers show the 90th and 10th percentiles. Outliers (extreme 5 percentiles) are represented with round markers. Inset: magnified region of small growth rates. For each condition, $n = 30$ independent measurements of individual growth events in 3 independent experiments.

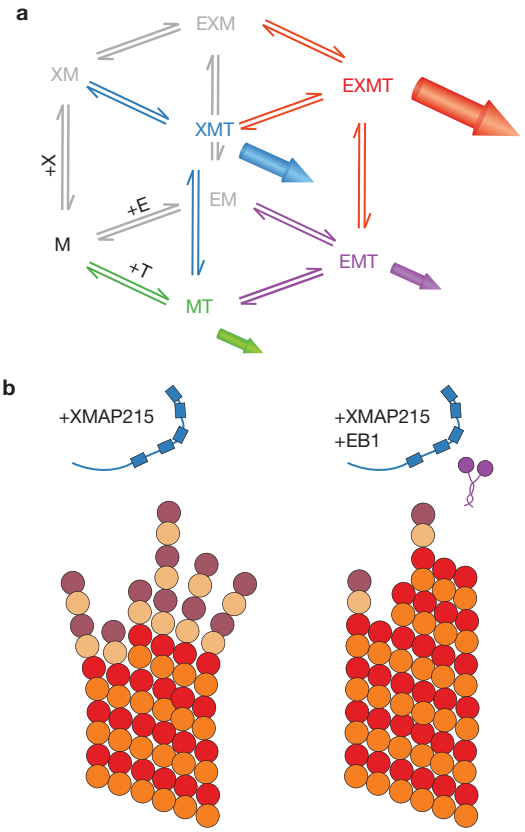

Figure 4 Model for catalysis of microtubule growth. (**a**) Reaction scheme for an enzymatic reaction with two non-essential activators. The microtubule end is viewed as an enzyme that catalyses the reaction: tubulin in solution (substrate) → tubulin in the polymer (product) by providing a much more efficient pathway than direct incorporation into the lattice. XMAP215 and EB1 are viewed as two non-essential enzyme activators that accelerate the net rate of addition at the end. Filled arrows represent the flux of polymerization through a particular vertex. M, microtubule end; T, free tubulin; X, XMAP215; E, EB1. (**b**) Microtubules growing in the presence of XMAP215 could have unstable elongated structures at protofilament ends (left, marked by different shading), which could be stabilized by the enhancement of lateral interactions by EB1, resulting in a straighter and blunter end structure (right).

taxol- and XMAP215-binding sites are on opposite sides of the tubulin dimer, the functional interaction is likely to be allosteric; likewise, we suggest that the synergy between EB1 and XMAP215 is also mediated allosterically through the tubulin protein.

To further investigate the mechanism underlying synergy we extended the existing model for the polymerase activity of XMAP215 (ref. 9) to include EB1. In this model, microtubule polymerization is viewed as an enzymatic reaction in which the microtubule end plays the role of an enzyme, free tubulin is the substrate and the polymerized tubulin is the product. XMAP215 is thought of as a non-essential enzyme activator, specifically promoting the formation of an intermediate complex in the polymerization reaction, which is a loosely bound tubulin dimer. By incorporating EB1 into this scheme, in a role of a second enzyme activator, we found that the polymerization rate in the presence of both activators (Fig. 4a, through vertex EXMT) is not simply given by the product of the rates when individual activators are present (through vertices XMT and EMT, for XMAP215 and EB1 alone, respectively). In other words, a purely catalytic scheme with no external energy source (such as GTP hydrolysis) can account for the observed synergy. Fitting our data to the model (see Methods) suggests that the observed boost in growth, when both EB1 and XMAP215 are present, is due to the promotion of the second reaction step, which is the isomerization of the loosely bound tubulin dimer into the stable microtubule lattice, consistent with our results obtained with taxol.

Our results provide reconstitution of physiological microtubule growth, with observed growth rates of 20 $\mu m\,min^{-1}$ that are at the upper end of the rates measured in cells[4–6]. Such growth rates have never previously been attained *in vitro*[2], and interestingly, they exhibit saturation with increasing tubulin concentration (Fig. 1c). Saturation has never been seen with either tubulin or actin polymerization, and is predicted by our catalytic model (see Methods). Even assuming simultaneous elongation of all of the 13 individual protofilaments, the observed growth rates correspond to an association rate constant for tubulin addition of up to 7.6 $\mu M^{-1}s^{-1}$ per protofilament, which is at the high end of the range of estimated maximum three-dimensional diffusion-limited rates of protein interactions (~1–10 $\mu M^{-1}s^{-1}$; refs 27, 28), and comparable to the association rate per protofilament of actin[29]. Recent work[30], using fluctuation analysis, estimated an association rate constant for the arrival of tubulin subunits similar to that measured here; in those experiments, however, net growth was much slower

owing to a high dissociation rate constant, such that only a small fraction of the arriving tubulin dimers are incorporated into the lattice. Thus, it is possible that in the presence of XMAP215 and EB1 almost all arriving dimers are incorporated into the lattice, yielding growth rates close to the maximum possible polymerization rate.

The observed fast microtubule growth rates are achieved in our assay through synergistic action of only two microtubule-associated proteins, XMAP215 and EB1, at the growing microtubule end. Recently, ref. 31 reported reconstitution of microtubule dynamics using *Drosophila* XMAP215, EB1 and another EB1-cargo protein, Sentin. However, growth rates achieved in that work were well below those observed in cells. Furthermore, the authors proposed that Sentin plays an important role in enhancement of microtubule growth. We show that neither Sentin nor any other proteins that bind XMAP215 and EB1 are necessary for promotion of microtubule growth to cellular rates. Thus, we have identified a minimal system needed for reconstitution of physiological microtubule growth.

Remarkably, both strong growth promotion and promotion of microtubule catastrophe are achieved simultaneously by the addition of EB1 to XMAP215 (Supplementary Fig. S1, black circles). This contrasts with XKCM1, which enhances catastrophe, but has no effect on growth rate in the presence of XMAP215 (ref. 2). Simultaneous promotion of growth and catastrophe is unexpected because many models of microtubule dynamic behaviour imply that a faster growth rate leads to a larger stabilizing structure at the dynamic microtubule end[32]. If the stabilizing structure is the GTP–tubulin cap[33], the observed simultaneous increase in microtubule growth rate and catastrophe frequency implies a coupled hydrolysis mechanism[34–36], in which the size of the stabilizing GTP cap is not very sensitive to the rate of addition of GTP–tubulin dimers. Unlike growth promotion, the promotion of catastrophe does not occur through a synergy with XMAP215; rather, it is an effect of EB1 alone. Our data obtained with taxol and modelling demonstrate that the polymerase activity of XMAP215 can be accelerated by inducing a structural change at the growing microtubule end. This structural change could involve straightening of the protofilaments[26] and changes in curvature of individual tubulin dimers[37,38] associated with strengthening of the lateral interactions between protofilaments[15,21,25,39]. The stabilization of lateral interactions by EB1 could accelerate GTP hydrolysis or phosphate release, thereby explaining the promotion of catastrophe. As EB1 binds only transiently at the microtubule end, it does not stabilize the microtubule, unlike taxol, which binds all along the microtubule lattice.

There are many occasions in the life of a cell when the microtubule network has to exhibit strong dynamicity to rapidly restructure itself. The behaviour of individual microtubules in the cell is governed by an intricate web of regulatory proteins associating with the exposed microtubule end. We find that even a simple interaction of two such proteins with the microtubule plus end leads to surprisingly complex behaviours, namely synergy of growth and high catastrophe, which may play an essential role for a large number of cellular processes. □

METHODS

Methods and any associated references are available in the online version of the paper.

Note: Supplementary Information is available in the online version of the paper

ACKNOWLEDGEMENTS

We thank M. Braun (MPI-CBG, Dresden, Germany) for the gift of EB1ΔC protein; S. Reber for help with protein expression and purification; M. Aliee, A. Clarke and M. Neetz, with whom this project was initiated as a part of the PhD programme course; G. Brouhard, S. Diez and M. Gardner for critical evaluation of the manuscript; and members of the Howard laboratory for discussions, reading and feedback. M.Z. was supported by a Cross-Disciplinary Fellowship from the International Human Frontier Science Program Organization. P.O.W. was supported by a European Molecular Biology Organization long-term fellowship.

AUTHOR CONTRIBUTIONS

M.Z., P.O.W., A.A.H. and J.H. designed research; M.Z. and P.O.W. performed research; M.Z. and J.H. analysed data; M.Z. and J.H. developed the theoretical model; M.Z., A.A.H. and J.H. wrote the paper.

COMPETING FINANCIAL INTERESTS

The authors declare no competing financial interests.

Published online at www.nature.com/doifinder/10.1038/ncb2744
Reprints and permissions information is available online at www.nature.com/reprints

1. Akhmanova, A. & Steinmetz, M. O. Tracking the ends: a dynamic protein network controls the fate of microtubule tips. *Nat. Rev. Mol. Cell Biol.* **9,** 309–322 (2008).
2. Kinoshita, K., Arnal, I., Desai, A., Drechsel, D. N. & Hyman, A. A. Reconstitution of physiological microtubule dynamics using purified components. *Science* **294,** 1340–1343 (2001).
3. Bieling, P. *et al.* Reconstitution of a microtubule plus-end tracking system *in vitro*. *Nature* **450,** 1100–1105 (2007).
4. Srayko, M., Kaya, A., Stamford, J. & Hyman, A. A. Identification and characterization of factors required for microtubule growth and nucleation in the early *C. elegans* embryo. *Dev. Cell* **9,** 223–236 (2005).
5. Komarova, Y. A. *et al.* Mammalian end binding proteins control persistent microtubule growth. *J. Cell Biol.* **184,** 691–706 (2009).
6. Stepanova, T. *et al.* History-dependent catastrophes regulate axonal microtubule behaviour. *Curr. Biol.* **20,** 1023–1028 (2010).
7. Bechstedt, S. & Brouhard, G. J. Doublecortin recognizes the 13-protofilament microtubule cooperatively and tracks microtubule ends. *Dev. Cell* **23,** 181–192 (2012).
8. Gard, D. L. & Kirschner, M. W. A microtubule-associated protein from Xenopus eggs that specifically promotes assembly at the plus-end. *J. Cell Biol.* **105,** 2203–2215 (1987).
9. Brouhard, G. J. *et al.* XMAP215 Is a processive microtubule polymerase. *Cell* **132,** 79–88 (2008).
10. Widlund, P. O. *et al.* XMAP215 polymerase activity is built by combining multiple tubulin-binding TOG domains and a basic lattice-binding region. *Proc. Natl Acad. Sci. USA* **108,** 2741–2746 (2011).
11. Bieling, P. *et al.* CLIP-170 tracks growing microtubule ends by dynamically recognizing composite EB1/tubulin-binding sites. *J. Cell Biol.* **183,** 1223–1233 (2008).
12. Dixit, R. *et al.* Microtubule plus-end tracking by CLIP-170 requires EB1. *Proc. Natl Acad. Sci. USA* **106,** 492–497 (2009).
13. Zanic, M., Stear, J. H., Hyman, A. A. & Howard, J. EB1 recognizes the nucleotide state of tubulin in the microtubule lattice. *PLoS ONE* **4,** e7585 (2009).
14. Niethammer, P. *et al.* Discrete states of a protein interaction network govern interphase and mitotic microtubule dynamics. *PLoS Biol.* **5,** e29 (2007).
15. Vitre, B. *et al.* EB1 regulates microtubule dynamics and tubulin sheet closure *in vitro*. *Nat. Cell Biol.* **10,** 415–421 (2008).
16. Blake-Hodek, K. A., Cassimeris, L. & Huffaker, T. C. Regulation of microtubule dynamics by Bim1 and Bik1, the budding yeast members of the EB1 and CLIP-170 families of plus-end tracking proteins. *Mol. Biol. Cell* **21,** 2013–2023 (2010).
17. Honnappa, S. *et al.* An EB1-binding motif acts as a microtubule tip localization signal. *Cell* **138,** 366–376 (2009).
18. Kronja, I., Kruljac-Letunic, A., Caudron-Herger, M., Bieling, P. & Karsenti, E. XMAP215-EB1 interaction is required for proper spindle assembly and chromosome segregation in Xenopus egg extract. *Mol. Biol. Cell* **20,** 2684–2696 (2009).
19. Gell, C. *et al.* Microtubule dynamics reconstituted *in vitro* and imaged by single-molecule fluorescence microscopy. *Methods Cell Biol.* **95,** 221–245 (2010).
20. Manna, T., Honnappa, S., Steinmetz, M. O. & Wilson, L. Suppression of microtubule dynamic instability by the +TIP protein EB1 and its modulation by the CAP-Gly domain of p150glued. *Biochemistry* **47,** 779–786 (2008).
21. Maurer, S. P., Fourniol, F. J., Bohner, G., Moores, C. A. & Surrey, T. EBs recognize a nucleotide-dependent structural cap at growing microtubule ends. *Cell* **149,** 371–382 (2012).
22. van der Vaart, B. *et al.* SLAIN2 links microtubule plus end-tracking proteins and controls microtubule growth in interphase. *J. Cell Biol.* **193,** 1–27 (2011).
23. Li, W. *et al.* EB1 promotes microtubule dynamics by recruiting Sentin in *Drosophila* cells. *J. Cell Biol.* **193,** 973–983 (2011).

24. Ayaz, P., Ye, X., Huddleston, P., Brautigam, C. A. & Rice, L. M. A TOG:-tubulin complex structure reveals conformation-based mechanisms for a microtubule polymerase. *Science* **337,** 857–860 (2012).
25. Georges, des, A. *et al*. Mal3, the *Schizosaccharomyces pombe* homolog of EB1, changes the microtubule lattice. *Nat. Struct. Mol. Biol.* **15,** 1102–1108 (2008).
26. Elie-Caille, C. *et al*. Straight GDP-tubulin protofilaments form in the presence of taxol. *Curr. Biol.* **17,** 1765–1770 (2007).
27. Northrup, S. H. & Erickson, H. P. Kinetics of protein–protein association explained by Brownian dynamics computer simulation. *Proc. Natl Acad. Sci. USA* **89,** 3338–3342 (1992).
28. Howard, J. *Mechanics of Motor Proteins and the Cytoskeleton* (Sinauer Associates, 2001).
29. Pollard, T. D. Rate constants for the reactions of ATP- and ADP-actin with the ends of actin filaments. *J. Cell Biol.* **103,** 2747–2754 (1986).
30. Gardner, M. K. *et al*. Rapid microtubule self-assembly kinetics. *Cell* **146,** 582–592 (2011).
31. Li, W. *et al*. Reconstitution of dynamic microtubules with *Drosophila* XMAP215, EB1, and Sentin. *J. Cell Biol.* **199,** 849–862 (2012).
32. Ranjith, P., Lacoste, D., Mallick, K. & Joanny, J.-F. Nonequilibrium self-assembly of a filament coupled to ATP/GTP hydrolysis. *Biophys. J.* **96,** 2146–2159 (2009).
33. Mitchison, T. J. & Kirschner, M. W. Dynamic instability of microtubule growth. *Nature* **312,** 237–242 (1984).
34. O'Brien, E. T., Voter, W. A. & Erickson, H. P. GTP hydrolysis during microtubule assembly. *Biochemistry* **26,** 4148–4156 (1987).
35. Walker, R. A. *et al*. Dynamic instability of individual microtubules analysed by video light microscopy: rate constants and transition frequencies. *J. Cell Biol.* **107,** 1437–1448 (1988).
36. Nogales, E., Wolf, S. G. & Downing, K. H. Structure of the alpha beta tubulin dimer by electron crystallography. *Nature* **391,** 199–203 (1998).
37. Rice, L. M., Montabana, E. A. & Agard, D. A. The lattice as allosteric effector: structural studies of alphabeta- and gamma-tubulin clarify the role of GTP in microtubule assembly. *Proc. Natl Acad. Sci. USA* **105,** 5378–5383 (2008).
38. Wang, H-W. & Nogales, E. Nucleotide-dependent bending flexibility of tubulin regulates microtubule assembly. *Nature* **435,** 911–915 (2005).
39. Prota, A. E. *et al*. Molecular mechanism of action of microtubule-stabilizing anticancer agents. *Science* **339,** 587–590 (2013).

DOI: 10.1038/ncb2744

METHODS

Protein preparation. Porcine brain tubulin was purified and labelled with TAMRA or Alexa Fluor 488 (Invitrogen) according to the standard protocols, as previously described[19]. Preparation of GMPCPP-stabilized microtubule seeds was performed as previously described[19]. XMAP215 and XMAP215–GFP were expressed in SF+ cells using the Bac-to-Bac system from Invitrogen and purified as previously described[10]. EB1 and EB1–GFP were expressed in *Escherichia coli* and purified as described previously[13]. The last 20 amino acids of EB1 were removed by directed site mutagenesis of the EB1–GFP construct and the stop codon was inserted in front of GFP to obtain the EB1ΔC construct. EB1ΔC was expressed in *E. coli* and purified using the same procedure as for EB1.

TIRF assay and imaging conditions. Assay for dynamic growth of Alexa488-labelled GTP–tubulin from tetrarhodamine-labelled GMPCPP-stabilized tubulin seeds imaged by TIRF microscopy was described previously[19]. The imaging buffer consisted of BRB80 supplemented with 40 mM glucose, 40 μg ml^{-1} glucose oxidase, 16 μg ml^{-1} catalase, 0.1 mg ml^{-1} casein, 50 mM KCl, 1% dithiothreitol and 1 mM GTP. Imaging was performed with an Andor iXon camera on a Zeiss Axiovert 200M microscope with a Zeiss ×100/1.45 α FLUAR objective and standard filter sets. An objective heater (Zeiss) was used to warm the sample to 35 °C. Image analysis was performed by creating kymographs of microtubule growth events in ImageJ. In the case of growth with free tubulin and EB1, microtubule polarity was determined using the processive plus-end-directed kinesin Kip3.

Size-exclusion chromatography. Size-exclusion chromatography was performed as previously described[10]. Concentrations of proteins used were 9 μM XMAP215 and 40 μM EB1 in the same buffer conditions as used in TIRF imaging assay (BRB80 supplemented with 50 mM KCl).

Reaction scheme with two non-essential enzyme activators. Microtubule polymerization in the presence of XMAP215 and EB1 can be thought of as an enzymatic reaction with two non-essential enzyme activators[40]. In this reaction scheme, the microtubule end (M) is viewed as the enzyme for the catalytic reaction of tubulin dimer (T) addition. XMAP215 and EB1 are two non-essential activators, denoted by X and E.

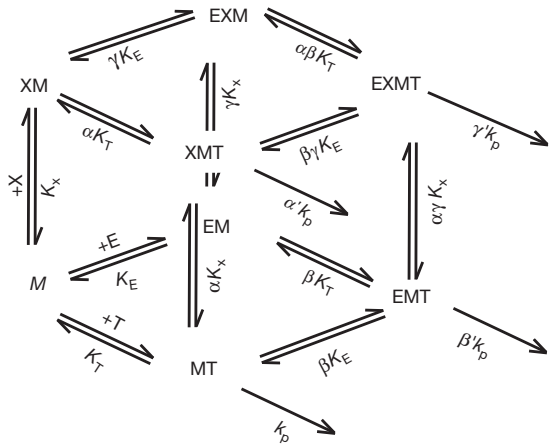

The polymerization reaction has two steps: formation of the intermediate state (MT) with a loosely bound tubulin dimer, followed by a slow isomerization reaction. The final product of the reaction is a tubulin stably incorporated into the microtubule lattice. The assumptions of the model are as follows: enzyme (M), substrate (T) and the intermediate product (MT) are in equilibrium; the amount of substrate (free tubulin, T) is much greater than the amount of enzyme (microtubule ends, M); the overall reaction rate is limited by the slow isomerization step; deisomerization is considered to be insignificant.

Note that the assumption that only early components of the reaction are at equilibrium is called quasi-equilibrium (or rapid equilibrium) and is valid only when the isomerization reaction is slow when compared with the decay of the intermediate state.

The full scheme leads to the following promotion of microtubule growth:

$$\frac{v}{[M]_t} = \left(k_p\frac{[T]}{K_T} + \alpha' k_p\frac{[X][T]}{\alpha K_X K_T} + \beta' k_p\frac{[E][T]}{\beta K_E K_T} + \gamma' k_p\frac{[X][E][T]}{\alpha\beta\gamma K_X K_E K_T}\right) \Big/ \left(1 + \frac{[X]}{K_X} + \frac{[E]}{K_E} + \frac{[T]}{K_T} + \frac{[X][T]}{\alpha K_X K_T} + \frac{[E][T]}{\beta K_E K_T} + \frac{[E][X]}{\gamma K_E K_X} + \frac{[X][E][T]}{\alpha\beta\gamma K_X K_E K_T}\right)$$

where $v/[M]_t$ is the reaction rate normalized by the total amount of enzyme (M); K_T, K_X and K_E are dissociation constants for the reactions of the microtubule end with free tubulin, XMAP215 and EB1, respectively. α, β and γ quantify the effect of either or both activators on the dissociation constant for the first reaction step (production of the intermediate state); k_p is the rate constant for the isomerization step, which is affected by the activators through coefficients α′, β′ and γ′.

The above equation shows that two non-essential activators in combination can act as a new activator, which activates the first step of the reaction with a factor αβγ, and the second step with a factor γ′. The synergistic behaviour of the activators becomes apparent owing to the fact that γ and γ′ can take any values, irrespective of the values of α, β, α′ and β′, which quantify the individual effects of the two activators.

When there are no activators present, the polymerization reaction with tubulin alone follows the standard Michaelis–Menten equation:

$$\frac{v}{[M]_t} = \frac{k_p([T]/K_T)}{1+([T]/K_T)} \tag{1}$$

Addition of one non-essential activator (XMAP215 or EB1), in the presence of tubulin, changes the velocity of the enzyme-catalysed reaction in the following way. Assume we have only XMAP215 (X) present. Then:

$$\frac{v}{[M]_t} = \frac{k_p([T]/K_T) + \alpha' k_p([X][T]/\alpha K_X K_T)}{1+([X]/K_X)+([T]/K_T)+([X][T]/\alpha K_X K_T)}$$

For a given [X], as $[T]\to\infty$, the growth rate is expected to reach a saturation level:

$$\frac{v}{[M]_t} \underset{[T]\to\infty}{\longrightarrow} \frac{k_p(1+\alpha'([X]/\alpha K_X))}{1+([X]/\alpha K_X)} \underset{[X]\to\infty}{\longrightarrow} \alpha' k_p$$

On the other hand, for saturating concentrations of the activator ($[X]\to\infty$), the growth rate is given by:

$$\frac{v}{[M]_t} \underset{[X]\to\infty}{\longrightarrow} \frac{\alpha' k_p([T]/\alpha K_T)}{1+([T]/\alpha K_T)}$$

which for small enough tubulin concentrations (well below the saturation limit) can be approximated by a linear relationship:

$$\frac{v}{[M]_t} \approx \alpha' k_p\frac{[T]}{\alpha K_T} \tag{2}$$

Similarly, with [E] alone the saturation in growth rates is achieved at high tubulin concentrations:

$$\frac{v}{[M]_t} \underset{[T]\to\infty}{\longrightarrow} \frac{k_p(1+\beta'([E]/\beta K_E))}{1+([E]/\beta K_E)} \underset{[E]\to\infty}{\longrightarrow} \beta' k_p$$

If only EB1 concentration is saturating, ($[E]\to\infty$), the growth rate is given by:

$$\frac{v}{[M]_t} \underset{[E]\to\infty}{\longrightarrow} \frac{\beta' k_p([T]/\beta K_T)}{1+([T]/\beta K_T)}$$

which for small enough tubulin concentrations (well below the saturation limit) can be approximated by a linear relationship:

$$\frac{v}{[M]_t} \approx \beta' k_p\frac{[T]}{\beta K_T} \tag{3}$$

With both [X] and [E], in the presence of tubulin, and for saturating concentration [X]:

$$\frac{v}{[M]_t} \underset{[X]\to\infty}{\longrightarrow} \frac{k_p(\alpha'([T]/\alpha K_T)+\gamma'([E][T]/\alpha\beta\gamma K_E K_T))}{1+([T]/\alpha K_T)+([E]/\gamma K_E)+([E][T]/\alpha\beta\gamma K_E K_T)} \tag{4}$$

which as $[T]\to\infty$:

$$\frac{v}{[M]_t} \underset{[T]\to\infty}{\longrightarrow} \frac{k_p(\alpha'+(\gamma'/\beta\gamma)([E]/K_E))}{1+([E]/\beta\gamma K_E)}$$

On the other hand, saturating concentrations of both [X] and [E] yield:

$$\frac{v}{[M]_t} \underset{[X],[E]\to\infty}{\longrightarrow} \frac{k_p\gamma'([T]/\alpha\beta K_T)}{1+([T]/\alpha\beta K_T)} \tag{5}$$

which as $[T]\to\infty$ saturates at a value of $k_p\gamma'$.

We now fit the appropriate model relationships, as derived above (equations (1), (2), (3) and (5)), to our experimental data in all four experimentally investigated cases (Supplementary Table S1). For growth rates obtained with tubulin alone, as well as with individual activators, the fits are done using the model predictions in the linear regime, as data show no indications of saturation. These three fits give:

$$\frac{k_p[M]_t}{K_T} = 0.094\,\mu m\,\mu M^{-1}\,min^{-1}$$

$$\frac{\alpha'}{\alpha}\frac{k_p[M]_t}{K_T} = 0.947\,\mu m\,\mu M^{-1}\,min^{-1} \quad (6)$$

$$\frac{\beta'}{\beta}\frac{k_p[M]_t}{K_T} = 0.118\,\mu m\,\mu M^{-1}\,min^{-1}$$

yielding the following relationships between parameters:

$$\frac{\alpha'}{\alpha} \approx 10, \quad \frac{\beta'}{\beta} \approx 1.3 \quad (7)$$

For the condition where both activators (XMAP215 and EB1) are used, a fit to the derived model prediction gives:

$$\gamma' k_p[M]_t = 40\,\mu m\,min^{-1} \quad (8)$$

$$\alpha\beta K_T = 8\,\mu M$$

yielding

$$\frac{\gamma'}{\alpha\beta} \approx 50 \quad (9)$$

Note also that the relationship derived for the case of two activators, one of which is at a saturating concentration (equation (4)), has the same functional form as the function used to fit the data in Fig. 1b:

$$v = v_0 + \frac{(v_{max} - v_0)[E]}{(K + [E])}$$

Indeed, the two relationships are identical given the following:

$$v_0 = \frac{k_p[M]_t\alpha'([T]/\alpha K_T)}{1 + ([T]/\alpha K_T)}$$

$$v_{max} = \frac{k_p[M]_t\gamma'([T]/\alpha\beta K_T)}{1 + ([T]/\alpha\beta K_T)}$$

$$K = \frac{\gamma K_E(1 + ([T]/\alpha K_T))}{1 + ([T]/\alpha\beta K_T)}$$

The fitted parameters are consistent with equations (6)–(9), and can be used to obtain a further prediction: $\gamma \approx 1$.

These relationships can be interpreted as follows. Note that the parameters denoted by prime symbols reflect the changes in the rate constant for the second, isomerization step, whereas the unprimed parameters affect the dissociation constant of the first reaction, formation of the intermediate, loosely bound tubulin state. An activator can affect either or both of these steps. For XMAP215, the model is that it promotes formation of the intermediate complex by decreasing the dissociation constant of the first step. Thus, the ratio between α and α' determined by our fit would be satisfied by: $\alpha = 0.1, \alpha' = 1$. EB1 on its own has a very mild effect on growth rate, which could be realized by both β and β' being close to 1. This then leads to a prediction: $\gamma' \approx 5$. In other words, EB1, when combined with XMAP215, is expected to strongly promote isomerization, the process of incorporation of the loosely bound tubulin dimer into the stable microtubule lattice.

40. Segel, I. H. *Enzyme Kinetics: Behavior and Analysis of Rapid Equilibrium and Steady State Enzyme Systems* (Wiley, 1975).

DOI: 10.1038/ncb2744

nature cell biology

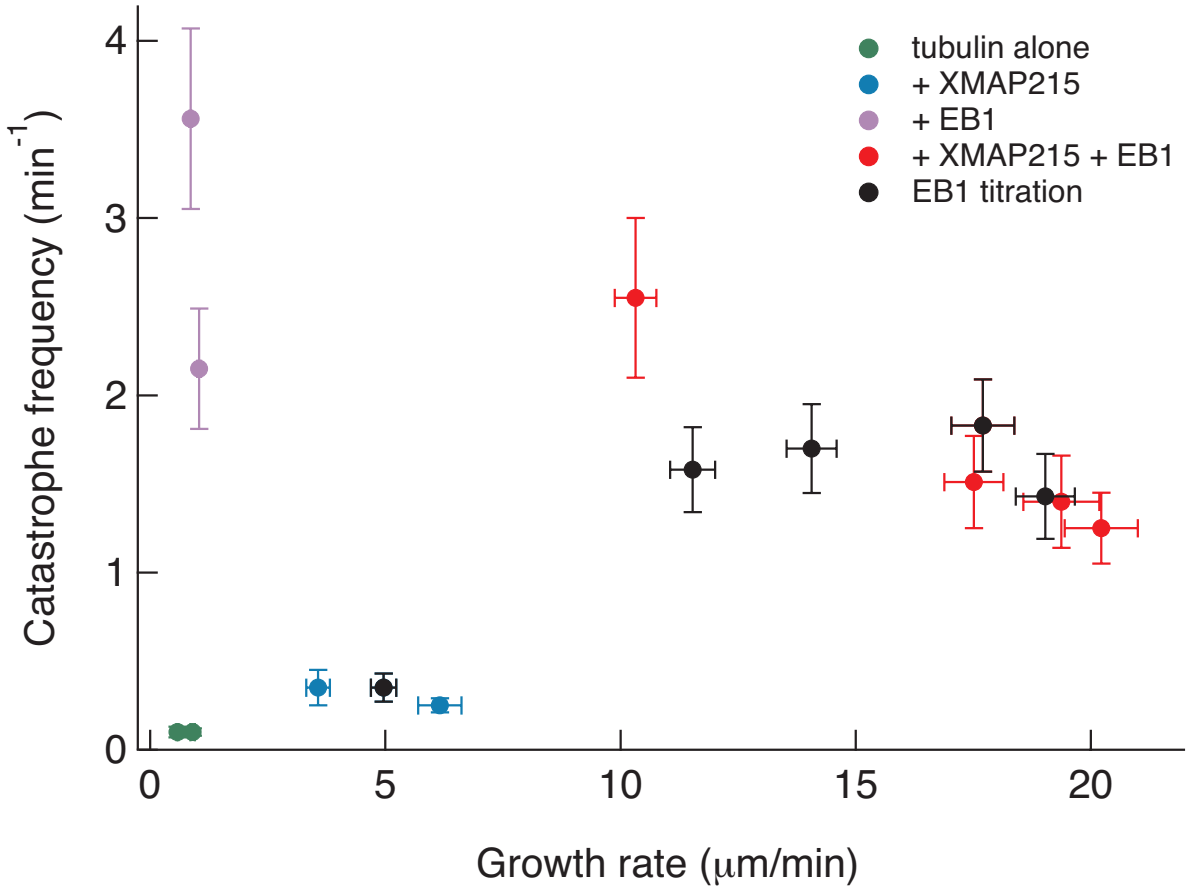

Figure S1 Catastrophe frequency is not a simple function of microtubule growth rate. Microtubule catastrophe frequency as a function of microtubule growth rate for: different EB1 concentrations in the presence of fixed amount of free tubulin (5 μM) and XMAP215 (200 nM) (black); a series of conditions involving different tubulin concentrations, a fixed amount of EB1 (400 nM) and/or XMAP215 (200 nM) (see Supplementary Table 1 for data). All error bars represent standard errors. EB1 titration (black): $N = (23, 20); (26, 44); (29, 47); (28, 48); (26, 36)$; Tubulin with XMAP215 and EB1 (red): $N = (18, 32); (28, 48); (27, 34); (18, 29); (32, 38)$; Tubulin with XMAP215 (blue): $N = (12, 12); (23, 20); (33, 31)$; Tubulin with EB1 (purple): $N = (19, 48); (30, 40)$; Tubulin alone (green): $N = (17, 15); (21, 18)$. The first number in parenthesis represents the number of independent measurements of individual growth events, and the second represents the number of observed catastrophe events. Two independent experiments were performed for 3 μM tubulin with XMAP215, and 3 μM tubulin with XMAP215 and EB1. Three independent experiments were performed for the remaining thirteen conditions.

Supplementary Table legends

Table S1 Microtubule dynamic instability parameters for different experimental conditions. The table lists microtubule growth and shrinkage rates, as well as catastrophe frequencies measured for a range of experimental conditions. For growth and shrinkage rates, N represents the number of independent measurements. For catastrophe frequency N represents the number of observed catastrophe events. Three independent experiments were performed for all conditions, except for the two conditions with 3 μM tubulin, for which two independent experiments were performed. Note that we do not report the frequency of rescues, as no rescues were observed in the above experimental conditions. *Lower limit determined due to the limitations in time resolution.

Table S2 Comparison of effects of full-length EB1 and EB1ΔC on microtubule growth rate and catastrophe frequency. The table lists microtubule growth rates and catastrophe frequencies measured in the presence of full-length EB1 or truncated EB1ΔC construct. For growth rates, N represents the number of independent measurements. For catastrophe frequency N represents the number of observed catastrophe events. Three independent experiments were performed for each condition.